Eur. Phys. J. D **28**, 149–154 (2004)
DOI: 10.1140/epjd/e2003-00287-1

THE EUROPEAN PHYSICAL JOURNAL D

# Experimental multi-photon-resolving detector using a single avalanche photodiode

O. Haderka[1,2,a], M. Hamar[2], and J. Peřina Jr[1,2]

[1] Joint Laboratory of Optics, Palacký University and Institute of Physics of Academy of Sciences of the Czech Republic, 17. listopadu 50, 772 07 Olomouc, Czech Republic
[2] Department of Optics, Palacký University, 17. listopadu 50, 772 07 Olomouc, Czech Republic

Received 10 March 2003 / Received in final form 16 July 2003
Published online 14 October 2003 – 

**Abstract.** A multichannel detector has been constructed using a single avalanche photodiode and a fiber-loop delay line. Detection probabilities of the channels can be set using a variable-ratio coupler. The performance of the detector is demonstrated on its capability to distinguish multi-photon states (containing two or more photons) from the one-photon state and the vacuum state.

**PACS.** 42.50.Dv Nonclassical states of the electromagnetic field, including entangled photon states; quantum state engineering and measurements – 03.67.Hk Quantum communication

## 1 Introduction

There is an increasing need for identifying the number of photons that is contained within a weak light pulse or time interval of a weak cw light field. A device capable of photon-number resolution would contribute both to fundamental research in the area of quantum optics and to more-or-less practical quantum communication systems, such as quantum key distribution schemes [1]. In the former case it would significantly help in the analysis and preparation of quantum states with prescribed photon-number statistics [2], in the latter it would prolong communication distances and increase the rate of secure communication [3–5]. A detector capable to resolve the vacuum state, one-photon Fock state and states containing more than one photon was recently constructed [6,7], but it requires operation under extreme conditions at present and it hardly becomes a common laboratory tool at least in near future. A similar problem occurs with a photon-number-resolving detector [8] based on superconducting transition-edge sensor microcalorimeter technology that needs mK temperatures for its operation.

Common detectors of weak light fields (avalanche photodiodes and photomultipliers) cannot provide photon-number resolution but they have high quantum efficiencies in the visible [9] and near infrared [10] regions. The use of a cascade of such detectors behind a $1\times N$ multiport [2,11] then provides a device capable to resolve photon-numbers to some extent. Assuming a lossless device, ideal detectors, and provided that the mean number of photons in the signal $\mu \ll N$, a part of any multi-photon signal containing $k$ photons gets split with a high probability to the arms of the multiport in such a way that $k$ detections at different detectors occur. (We note that in the limit $N \to \infty$ this probability is one.) However, it was shown in [2] that the performance of such device is severely inflicted by losses in the device and imperfections of the detectors. To achieve a reasonable performance, a large array of detectors with high quantum efficiency and low noise is required [2], so that such photon-number-resolving device becomes unacceptably complex. Recently, photon-number-resolving detectors having 8 or 16 nearly balanced channels and utilizing 2 single-photon detectors together with time multiplexing have been constructed [12,13]. They represent a practically achievable alternative of the scheme based on a symmetric $1 \times N$ multiport. The use of this photon-number-resolving device in a source of one-photon Fock states based on entangled photon pairs and postselection was analyzed in [4]. It was shown that photon fields with the Fano factor around 0.7 can be generated by this source under real conditions. A quantum-key distribution system using this source can have a secure communication distance up to 120 km and can provide higher values of gain [4]. These results motivate the endeavour to simplify the above discussed photon-number-resolving device. We note that also single-photon sources utilizing NV centers [14] and quantum dots [15–17] are perspective for quantum-key distribution systems. However, NV centers have low efficiencies of single-photon generation ($\approx 10^{-3}$) and quantum-dot sources have to be cooled to 5 K at present.

In this paper we propose and test a variant of such cascading device in which we replace the $1 \times N$ multiport and $N$ detectors with a fiber-loop delay line and a single avalanche-photodiode detector. This decreases the complexity as well as the cost of the device to a reasonable

[a] e-mail: haderka@sloup.upol.cz

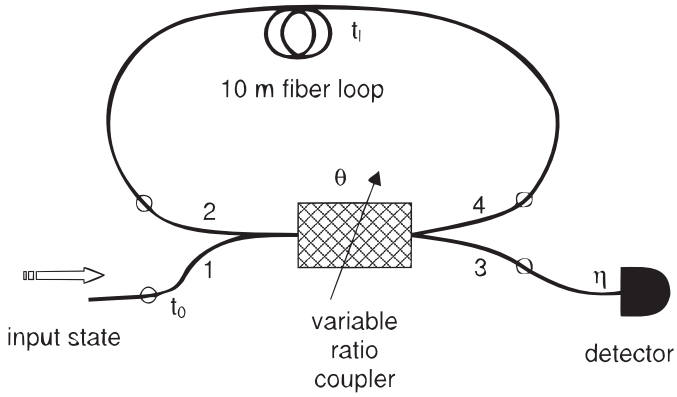


**Fig. 1.** Scheme of the device. Incoming quantum state is fed to input 1 of the variable ratio coupler (SVR). Detector is connected to pigtail 3. Pigtails 2 and 4 are connected with a 10 m long fiber patchcord that serves as a delay line. All pigtails of the SVR are 1 m long. Circles denote FC connectors.

measure. A similar device has been recently suggested also by other authors [18]. The number of detectors $N$ is given by the number of time windows (channels) we detect using the time-of-flight spectrometer. We use a variable-ratio coupler at the entrance to the fiber-loop delay line so that we can control the distribution of probabilities of detection in the individual channels. In order to show the performance of this fiber-loop detection device, we theoretically determine and experimentally test the best setting of the device with respect to distinguishing multi-photon states (containing two or more photons) from the one-photon state and the vacuum state.

## 2 Description of the device

The scheme of our device is plotted in Figure 1. Quantum state to be analyzed is injected to port 1 of the single-mode variable ratio coupler (SIFAM SVR-82, referred as SVR hereafter). Port 3 outputs to a detector module based on a silicon avalanche photodiode with active quenching (Perkin-Elmer SPCM-AQ-141-FC). This detector yields TTL output upon incident photon with quantum efficiency $\eta$ of 60% (at 830 nm, including coupling-optics losses) and is not capable of resolving the number of incident photons. The dark count rate is about 40 counts per second. Ports 2 and 4 are interconnected with 10 m long single-mode fiber thus forming a delay line longer than the dead time of the detector which is 50 ns. The outputs of the detector are registered as stop pulses in the time-of-flight spectrometer (Fast ComTec TOF7885) that is connected to a PC directly or through a multichannel buffer. Start pulses for the time-of-flight spectrometer are generated by trigger pulses of the source of quantum states to be examined.

Denoting the intensity transmission coefficients from port $i$ to port $j$ of the SVR by $t_{ij}$, the device input coupling transmission by $t_0$ (due to loss at the input connector), the SVR transmission by $\theta$ (due to SVR excess loss), the total transmission of the fiber loop by $t_l$ and the transmission from port 3 of the SVR to the detector including detector quantum efficiency by $\eta$, we arrive at the transmission coefficients $h_1, h_2, ...$ for the detection channels:

$$h_1 = t_0 \theta t_{13} \eta, \tag{1}$$

$$h_k = t_0 t_{14} \theta^k t_l^{k-1} t_{23} t_{24}^{k-2} \eta, \quad k \geq 2. \tag{2}$$

If a single photon enters the device, transmission coefficients give also the probabilities of photon detection.

A question arises, what is the optimum setting of the SVR for the detection of multi-photon states. The highest probability to distinguish multi-photon states from the one-photon state and the vacuum state is achieved provided that the probabilities $h_1, ..., h_N$ have the same value. The reason is that the energy in a detected photon field is equally distributed over all detectors and then the intensities of the photon fields in all detectors reach the lowest possible value. This case can be also distinguished by maximizing Shannon entropy. We cannot reach this best case with our fiber-loop detection device. Best conditions from the point of view of photon-number resolution obtainable by our fiber-loop detection device can be found only numerically in principle. However, numerical calculations as well as experimental results indicated that the principle of maximization of Shannon entropy is valid for this task and can provide these conditions (see Fig. 4).

We first simplify the real SVR to an idealized unitary device setting $\theta = t_0 = 1$, $t_{13} + t_{14} = 1$, $t_{23} + t_{24} = 1$, and $t_{13} + t_{23} = 1$. This idealized coupler can then be represented with a single variable-division-ratio parameter $r$. Upon replacing $t_{13} = t_{24} \to r$ and $t_{14} = t_{23} \to (1 - r)$ we get:

$$h_1 = \eta r, \tag{3}$$

$$h_k = \eta (1 - r)^2 t_l^{k-1} r^{k-2}, \quad k \geq 2. \tag{4}$$

Assuming further $t_l = \eta = 1$ in the ideal case, we can evaluate Shannon entropy

$$E = -\sum_i h_i \ln(h_i) \tag{5}$$

of the ideal channel detector as follows:

$$E = -2r \ln(r) - 2(1 - r) \ln(1 - r). \tag{6}$$

This entropy is maximized for $r = 1/2$, i.e., a balanced SVR is optimal. In the more general case $0 < t_l, \eta, \theta < 1$ the condition for maximum entropy needs to be evaluated numerically and it can be found that for realistic values of $t_0, t_l, \eta$, and $\theta$ the maximum value of entropy is decreased and the maximum occurs for $r < 1/2$. Thus, in a real device we can expect best performance of the detector when SVR is unbalanced in favor of port 4. For the parameters of our device we get the maximum value of entropy at $r = 0.446$.

## 3 Experimental results

For an experimental test of the detector we have fed it with a source of faint laser pulses with Poissonian statistics and

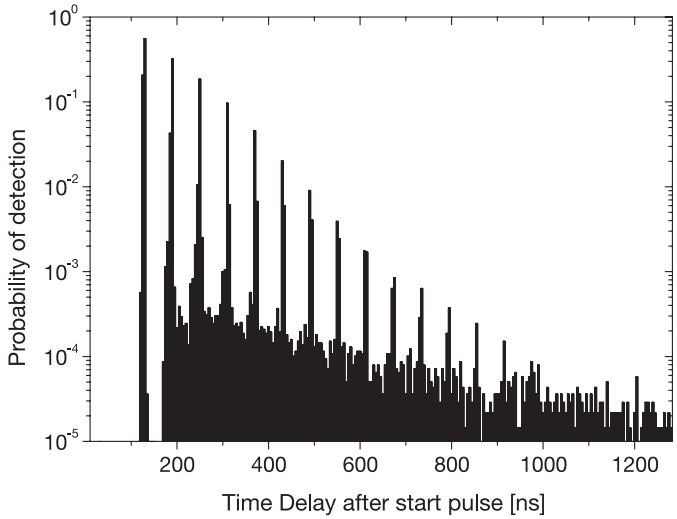


**Fig. 2.** A typical time spectrum obtained using the time-of-flight spectrometer at the mean photon number $\mu \doteq 2.13$. The spectrum is shown as a histogram of probabilities of detection per time bin; 1024 bins by 5 ns have been registered. Please note the logarithmic scale.

variable mean photon number. They have been obtained from a laser diode (SHARP LT015) yielding 4 ns pulses that have been subsequently attenuated by a digital variable attenuator (OZ Optics DA-100) to a single-photon level.

A typical time spectrum measured by the time-of-flight spectrometer at the mean photon number $\mu \doteq 2.13$ (see Eq. (10) below for the definition of $\mu$) is shown in Figure 2. Multiple peaks can be resolved at time distances of about 60 ns. The background between the peaks is caused by afterpulses, i.e. false detections that occur after dead time of the detector. This is why they are not present between the first two peaks. In our detector, the total afterpulse probability is of the order of $p_{ap}^{\mathrm{peak}} \approx 8 \times 10^{-3}$. The envelope of the afterpulse probabilities coming from individual peaks then forms the background pattern visible in Figure 2. At low intensities the probability of detection due to an afterpulse is considerably lower so that the main source of noise are the dark counts of the detector whose probability is $2 \times 10^{-7}$ per 5 ns bin.

The use of multiple time windows limits the repetition rate of the fiber-loop detector. The number of useful channels (those that have signal-to-noise ratios higher than 1) is limited to 15 in our case and then the total measurement period takes about 900 ns. This gives a maximum possible repetition rate of 1.1 MHz. However, the repetition rate has been limited to 100 Hz by the speed of time-of-flight spectrometer in our experimental setup. Nevertheless, repetition rate of 1 MHz can be achieved with custom-made electronics.

It is important to know the losses in the device. The total transmission of the device may be evaluated using equations (1) and (2) as

$$T = \sum_{k=1}^{\infty} h_k = \eta t_0 \left[ \frac{\theta(t_{13}t_{24} - t_{14}t_{23})}{t_{24}} - \frac{t_{14}t_{23}\theta}{t_{24}(t_l t_{24}\theta - 1)} \right]. \tag{7}$$

The quantity $T/\eta$ can be measured directly and we have found $T/\eta = 0.78 \pm 0.01$. Since $\eta$ is specified by the manufacturer of the detector, the total transmission $T$ of the device is known. However, upon inspecting equation (7) we can get more insight into the structure of the losses.

We have observed experimentally that the total transmission $T$ depends only weakly on the SVR setting. We therefore again replace the four $t_{ij}$ coefficients by a single parameter $r$ and arrive at a simplified expression

$$T \approx \frac{\eta t_0(2t_l\theta - 1)}{t_l} - \frac{\eta t_0(t_l\theta - 1)^2}{t_l(r t_l\theta - 1)}. \tag{8}$$

Since the dependence of $T$ on $r$ is weak, we may deduct that $T$ is given dominantly by the first term in equation (8). The value of $\theta$ was found in an independent measurement to be $\theta = 0.955$. The transmission of the fiber loop $t_l$ can be found from the measured values of the normalized channel probabilities $H_k = h_k/T$ ($\sum_{k=1}^{\infty} H_k = 1$). In particular, the ratio $H_{k+1}/(H_k H_1)$ evaluates to

$$\frac{H_{k+1}}{H_k H_1} \approx 2\theta t_l - 1, \tag{9}$$

where only the first term of equation (8) has been used. From experimental results we find the value $H_{k+1}/(H_k H_1) \approx 0.80$ to be almost independent of $r$ and $k$ (thus justifying the approximations used). From equation (9) we then get $t_l \approx 0.94$ (0.27 dB). Finally, the value of input coupling transmission $t_0$ is evaluated from equation (8) as $t_0 \approx 0.92$ (0.36 dB). These values are rather low and are caused mainly by the wear-out of the connectors used in our laboratory setup. The application of new connectors or fused fibers would further improve the performance of the device.

The division ratio of the SVR is set by a micrometer screw. The distribution of detection probabilities to the first six channels based on the SVR position is shown in Figure 3. The small white area in the top part of the plot corresponds to the sum of the higher channels ($k > 6$). We can see that various settings are possible. We can, e.g., set the device to the regime of one dominant channel with other channels weak but a moderate number of them (5 or 6) non-negligible (their weight is above 1%; see positions 5–10 in Fig. 3), or to a different regime of fewer but relatively balanced channels (see, e.g., position 19 in Fig. 3 where the first three channels are in the ratio 39%:42%:13%).

Let us now have a look at the capability to resolve multi-photon states using our device. We characterize the measured Poissonian signal by the mean photon number $\mu$. The mean photon number $\mu$ is obtained from the measured probability of detection $p$ assuming detection of the whole Poissonian signal by the detector

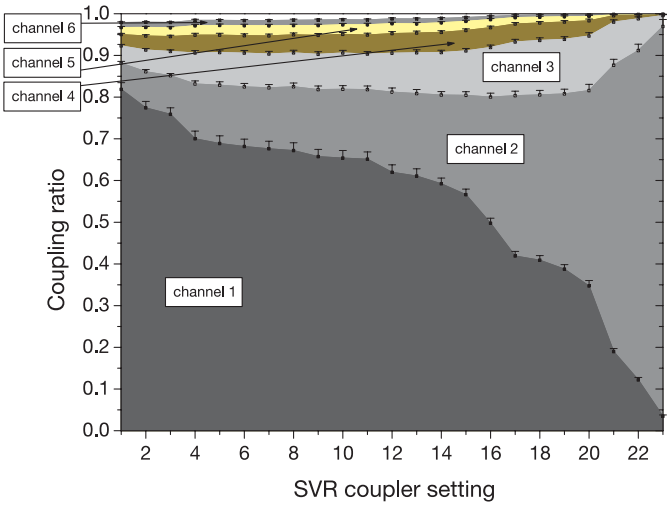


**Fig. 3.** Division ratio of the first six channels of the multichannel detector based on the SVR setting. The tick labels at $x$-axis roughly correspond to the scale of the micrometer screw.

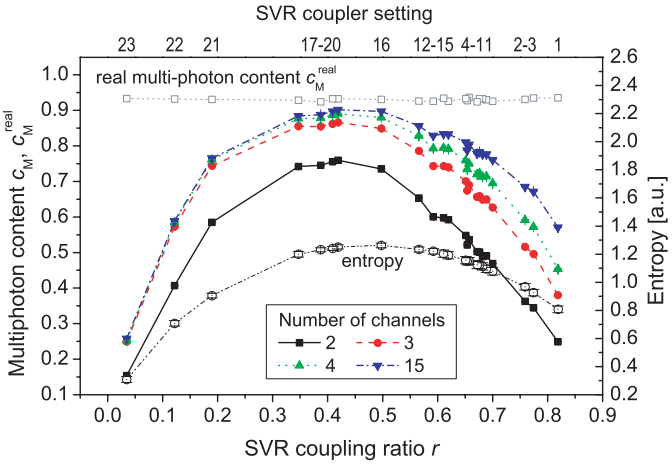


**Fig. 4.** Dependence of the multi-photon content $c_M$ on the SVR setting given by $r$ when detected by 2, 3, 4, and 15 channels of the device (see inset legend). A real multi-photon content $c_M^{\mathrm{real}}$ in the coherent state in front of the device (dotted line with open rectangles) is shown for comparison. The mean pulse energy $\mu$ of the input state was 4.26 photons per pulse. The dash-dot line with open circles is Shannon entropy determined from the measured division ratios of the first 15 channels.

with efficiency $T$, for which $p = \sum_{i=1}^{\infty} p_n = 1 - p_0 = 1 - \exp(-T\mu)$, i.e.

$$\mu = -\ln(1-p)/T. \tag{10}$$

Our measured signal had $\mu$ equal to 4.26 photons per pulse. The probability of vacuum state detection $p_0$, single-channel detection $p_1$, and multichannel detection $p_M = \sum_{k=2}^{\infty} p_k$ were extracted from the measured data. At each setting, the probabilities were obtained by detecting large number of laser pulses ($\sim 10^5$). We characterize the fraction of multi-photon states detected by our detector with another quantity, namely the multi-photon content $c_M$,

$$c_M = p_M/(p_1 + p_M) \tag{11}$$

($c_M$ gives the probability that non-vacuum pulses contain more than 1 photon) [4]. Figure 4 shows the multi-photon content $c_M$ detected with our device at the mean photon number $\mu = 4.26$ photons per pulse. For comparison, a real multi-photon content $c_M^{\mathrm{real}}$ (computed from Eq. (11) where $p_1$ and $p_M$ are given by Poissonian distribution with $\mu = 4.26$) in a Poissonian laser pulse in front of the device is shown as well ($c_M^{\mathrm{real}}$ is not constant in Fig. 4 because the laser intensity slightly fluctuated in the course of measurement). The highest values of detected $c_M$ have been observed for SVR positions 16–20 with maximum at position 17. The value of detected $c_M$ grows with the number of channels considered. Due to losses in the device and limited quantum efficiency of the detector, the measured multi-photon content $c_M$ is lower than the real multi-photon content $c_M^{\mathrm{real}}$. Nevertheless, the value of the measured multi-photon content $c_M$ was lower by less than 4% in comparison with the value of the real multi-photon content $c_M^{\mathrm{real}}$ at best performance of the device (SVR position 17, 15 channels) for this pulse-energy level. It is also worth noting that the use of a larger number of channels may be useful in the regime with the first dominant channel while it brings only a negligible improvement in case of fewer but relatively balanced channels. This is due to the fact that in the latter regime the total energy detected by the weakly exposed channels is much lower than in the regime with the first dominant channel. Values of entropy for each setting of the SVR are also plotted in Figure 4 and they clearly show that entropy of the multichannel detector provides the right indication of the multi-photon-resolution capability. The optimum performance of the device is achieved close to the value $r = 0.453$ as estimated theoretically in the preceding section.

Curves contained in Figure 4 suggest the use of three relatively balanced channels for a practical application. The multi-photon content $c_M$ is detected with the probability around 85% in this case. This performance is better than that obtainable with a comparably complex detection device based on a $1\times2$ beamsplitter and two detectors at its outputs; this device would identify the multi-photon content $c_M$ with the probability around 80%. We note that the higher the multi-photon content in the measured signal, the better the profit obtained from using multiple detection channels.

The performance of the detector in identification of the multi-photon content over a wide range of the mean photon number $\mu$ of the input Poissonian state is shown in Figure 5. The measured values of the multi-photon content $c_M$ (black rectangles) follow closely the (dashed) curve of the real multi-photon content $c_M^{\mathrm{real}}$ of the input state. The ratio of the measured values of the multi-photon content $c_M$ to the real ones given by $c_M^{\mathrm{real}}$ determines the efficiency of identification of multi-photon states and is also shown in Figure 5. It can be seen in Figure 5 that the ratio exceeds 60% for weak coherent states and reaches almost unity for strong coherent states.

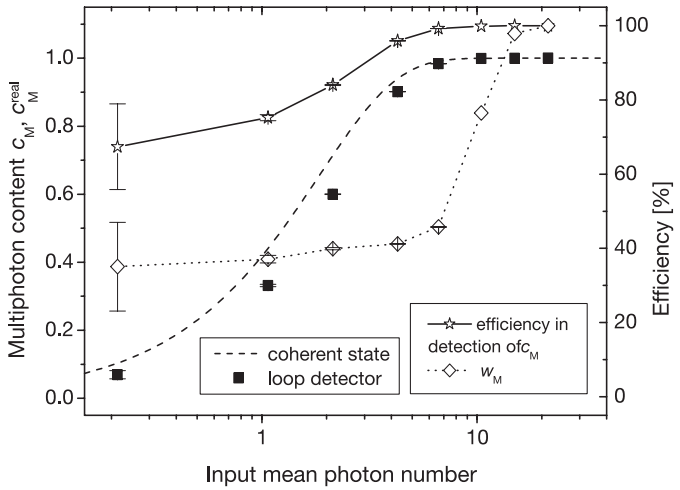


**Fig. 5.** Dependence of the measured multi-photon content $c_M$ (black rectangles) on the mean photon number $\mu$ of the input coherent state when detected with 15 channels of the device. The real multi-photon content $c_M^{\mathrm{real}}$ of the input state is shown by the dashed curve. Solid curve with stars (right axis) gives the ratio of the measured value of $c_M$ to the real one $c_M^{\mathrm{real}}$. The dotted curve with hollow diamonds (right axis) gives the ratio $w_M$ (for the definition, see text below).

Reduction of the multi-photon content $c_{M,\mathrm{in}}$ of a beam can be reached in the following scheme. A source provides perfectly correlated photon pairs (e.g., such pairs are generated by spontaneous parametric downconversion). One of the correlated beams is postselected by the measurement on the other beam using our fiber-loop detection device. Postselection process provides a beam with lower values of the multi-photon content $c_{M,\mathrm{out}}$. The ratio $w_M$ ($w_M = c_{M,\mathrm{out}}/c_{M,\mathrm{in}}$) then determines efficiency of this reduction. The dependence of the ratio $w_M$ on the mean photon number $\mu$ in Figure 5 shows that the value of the ratio $w_M$ can be reduced down to 40% for input Poissonian states with $\mu \leq 5$. The most interesting input states for applications utilizing multi-photon reduction are those containing a more-or-less balanced mixture of vacuum, single-photon and multi-photon contributions. The reason is that weak Poissonian states contain only a small fraction of multi-photon states (e.g., $c_M \approx 0.005$ for $\mu = 0.01$) whereas the fraction of a one-photon state is practically negligible in strong coherent states. The reduction down to 40% can be ideally reached for such states. We note that a real source would be characterized by higher values of the ratio $w_M$ due to imperfect coupling of photons in a pair [4].

It should be mentioned that in fact our measured value of the multi-photon content is slightly influenced by the noises in the device. The noise counts may cause multichannel detection even when only a single photon from the laser pulse has been detected. It is difficult to determine exactly the contribution of these false multi-detections. However, it is possible to estimate the upper limit of false detections due to afterpulses as $p_M^{\mathrm{false}} < p_1 p_{ap}^{\mathrm{peak}} q$, where $q$ is a duty factor of the detector channels at the time-of-flight spectrometer (i.e., the ratio of the channel time window to the time distance between channels; $q = 0.17$ in our case). Then the contribution to the multi-photon content due to afterpulses $c_M^{\mathrm{false}} < p_{ap}^{\mathrm{peak}} q \approx 1.4 \times 10^{-3}$. For very weak pulse energies false multiple detections might rather stem from dark counts of the detector. Nevertheless, the latter would become notable only at mean-photon-number levels below $10^{-5}$ photon per pulse. Therefore, the influence of noises is negligible in our device.

The analyzed device might help in the preparation of photon-number-squeezed states by postselection from entangled photon pairs obtained by spontaneous parametric downconversion [4]. Vacuum states can easily be filtered out similarly to the case of postselection with a single detector [3] and the fraction of multi-photon states can be significantly reduced using multichannel detection. The obtained states are potentially useful, e.g., for quantum-key distribution systems. Our device is a cheap, though not better in performance, alternative to the cascading detector [2,12,13] for this purpose. Other devices like those based on NV centers, quantum dots or using detectors with a superconducting microcalorimeter are quite demanding even for a common laboratory practice, at least at present.

In this work we use only the information whether single or multiple detections occurred regardless of the information in which channels the photons were detected. Since the channels exhibit different detection probabilities, there is an additional information which might be used. In general, it is possible to obtain the photon-number statistics of a detected quantum state to some extent [19].

In conclusion, we have built a configurable multichannel detector using a single avalanche photodiode. We have characterized the best regimes for its operation as multi-photon-resolving detector. Our analysis shows, that this device can efficiently distinguish multi-photon states from the one-photon state and the vacuum state over a wide range of energies of the input state.

The authors acknowledge the support by the projects Research Center for Optics (LN00A015), CEZJ-14/98 and RN19982003013 of the Ministry of Education of the Czech Republic. Support from the EU grant under QIPC, Project No. IST-1999-13071 (QUICOV) is also acknowledged. The authors thank Pavel Trojek for his contribution to the experimental setup.

## References

1. For a recent review see N. Gisin, G. Ribordy, W. Tittel, H. Zbinden, Rev. Mod. Phys. **74**, 145 (2002)
2. P. Kok, S.L. Braunstein, Phys. Rev. A **63**, 033812 (2001)
3. G. Brassard, N. Lütkenhaus, T. Mor, B.C. Sanders, Phys. Rev. Lett. **85**, 1330 (2000)
4. J. Peřina Jr, O. Haderka, J. Soubusta, Phys. Rev. A **64**, 052305 (2001)
5. Z. Walton, A.V. Sergienko, M. Atatüre, B.E.A. Saleh, M.C. Teich, J. Mod. Opt. **48**, 2055 (2001)

6. J. Kim, S. Takeuchi, Y. Yamamoto, H.H. Hogue, Appl. Phys. Lett. **74**, 902 (1999)
7. S. Brattke, B.T.H. Varcoe, H. Walther, Phys. Rev. Lett. **86**, 3534 (2001)
8. A.J. Miller, S.W. Nam, J.M. Martinis, A.V. Sergienko, Appl. Phys. Lett. **83**, 791 (2003)
9. S. Cova, M. Ghioni, A. Lacaita, C. Samori, F. Zappa, Appl. Opt. **35**, 1956 (1996)
10. G. Ribordy, J.D. Gautier, H. Zbinden, N. Gisin, Appl. Opt. **37**, 2272 (1998)
11. H. Paul, P. Törmä, T. Kiss, I. Jex, Phys. Rev. A **56**, 4076 (1997)
12. D. Achilles, Ch. Silberhorn, C. Sliwa, K. Banaszek, I.A. Walmsley, `quant-ph/0305191`
13. M.J. Fitch, B.C. Jacobs, T.B. Pittman, J.D. Franson, `quant-ph/0305193`
14. Ch. Kurtsiefer, S. Mayer, P. Zarda, H. Weinfurter, Phys. Rev. Lett. **85**, 290 (2000)
15. Ch. Santori, M. Pelton, G. Solomon, Y. Dale, Y. Yamamoto, Phys. Rev. Lett. **86**, 1502 (2001)
16. M. Pelton, Ch. Santori, J. Vuckovic, B. Zhang, G.S. Solomon, J. Plant, Y, Yamamoto, Phys. Rev. Lett. **89**, 233602 (2002)
17. R.M. Stevenson, R.M. Thompson, A.J. Shields, I. Farrer, B.E. Kardynal, D.A. Ritchie, M. Pepper, Phys. Rev. B **66**, 081302(R) (2002)
18. K. Banaszek, I.A. Walmsley, Opt. Lett. **28**, 52 (2003); `quant-ph/0206162`
19. J. Řeháček, Z. Hradil, O. Haderka, J. Peřina Jr, M. Hamar, Phys. Rev. A **67**, 061801(R) (2003)